Evaluation of liquefaction strength curves using energy dissipation

Evaluation de courbes des forces de liquéfaction utilisant la dissipation d'énergie

Tsuyoshi Honda, Yoshimasa Shigeno
Research & Development Institute, Takenaka Corporation, Japan, honda.tsuyoshi@takenaka.co.jp

ABSTRACT: The liquefaction strength curves defined as a relationship between the numbers of cycles and cyclic stress ratios make an important role in predicting a risk of liquefaction due to an irregular seismic load. This paper conducted a series of cyclic undrained triaxial tests and tried to obtain a liquefaction strength curve from a single specimen using the concept that the dissipation energy calculated from stress-strain loops was constant until liquefaction occurred. Using the stress ratios and the normalized dissipation energy divided by confining pressures at the beginning of each cycle, a particular relationship between the stress ratios and the increments of normalized dissipation energy was obtained as well as that of excess pore pressure and the normalized energy dissipation. The procedures to obtain a liquefaction strength curve from a single test were proposed using the two particular relationships, and were verified from the results of cyclic undrained triaxial tests.

RÉSUMÉ : Les courbes de forces de liquéfaction, définies comme une relation entre le nombre de cycles et les taux de stress cycliques jouent un rôle important dans la prédiction de la liquéfaction due à des charges sismiques irrégulières. Cette étude rapporte une série de tests triaxiaux cycliques sans drainage, pour tenter d'obtenir une courbe des forces de liquéfaction à partir d'un spécimen unique; basée sur le concept que l'énergie dissipée, calculée à l'aide de boucles induites par le stress, reste constante jusqu' l'apparition de la liquéfaction. Utilisant les taux de stress et la dissipation d'énergie normalisée, divisées par les pressions confinées au début de chaque cycle, nous avons obtenu tout d'abord une relation particulière entre les taux de stress et des incréments de la dissipation d' énergie normalisée et aussi une relation entre les pressions excessives des pores et la dissipation d'énergie normalisée. Les procédés d'obtention de la courbe de liquéfaction à partir d'un test unique sont proposées ici, par utilisation de ces deux relations particulières et nous les avons vérifiées avec les résultats de tests triaxiaux cycliques sans drainage.

KEYWORDS: energy dissipation, liquefaction strength curve, sand.

1 INTRODUCTION

The liquefaction strength curves defined as a relationship between the numbers of cycles and cyclic stress ratios make an important role in evaluating liquefaction potential and predicting liquefaction-induced damage due to an irregular seismic load. However, they were hardly measured in many projects, since it took much cost and time to collect several specimens with the same properties from an inhomogeneous ground, and execute several loading tests with different cyclic stress ratios. The dissipation energy calculated from stress-strain loops has a good correlation with the development of excess pore pressure during cyclic undrained loads (Towhata and Ishihara 1985). It has an advantage in evaluating liquefaction resistance and a ductility from a stress-strain behavior of single specimen (Kazama et. al. 2000). Kokusho and Mimori 2015 demonstrated the validity of the energy-based method using the dissipation energy in evaluating liquefaction potential during an earthquake. But many practical engineers have not been accustomed to the energy-based method. The stress-based method using safety factors of liquefaction strengths to cyclic stress ratios has been stereotypically used in many projects, though the stress-based method is not always accurate in predicting liquefaction during an earthquake.

From a viewpoint of practical engineers, the authors conducted a series of cyclic undrained triaxial tests, and proposed a new method to obtain a liquefaction strength curve from a single specimen using the dissipation energy.

2 CYCLIC UNDRAINED TRIAXIAL TESTS

Iide silica sand was used in cyclic undrained triaxial tests, the grain size distribution curve and physical parameters of it were shown in Figure 1. The specimens with a relative density of 70% were prepared by a wet tamping method. They were saturated using carbon dioxide gas and were isotopically consolidated with a confining pressure of 100 kPa.

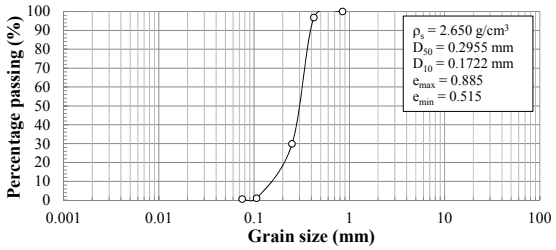

Figure 1. Grain size distribution curve of Iide silica sand (No.6).

Table 1. Test parameters and results in the cyclic undrained triaxial tests.

Case	No.1	No.2	No.3	No.4
γ_t (kN/m^3)	19.80	19.82	19.78	19.79
e	0.618	0.615	0.620	0.618
D_r (%)	72.2	73.0	71.6	72.2
V_p (m/s)	2010	2010	2010	2011
V_s (m/s)	217	187	214	205
ν	0.494	0.496	0.494	0.495
τ/σ'_c	0.293	0.245	0.202	0.210
$N_{c,\Delta u=95\%}$	11	14	47	32

Cyclic loading tests were carried out using a frequency of 0.1 Hz and cyclic stress ratios (CSR) from 0.201 to 0.249. Table 1 shows the physical properties of specimens after the consolidation, the cyclic stress ratios and the numbers of cycle reaching 0.95 in the excess pore pressure ratio. In Table 1, the velocities of P and S waves in the vertical direction of

specimens were measured to check an identity of the specimens. Poisson's ratios were also calculated from them. While the velocity of S wave had slightly higher scatter, the other properties were almost same in all the specimens.

3 RESULTS AND DISCUSSIONS

Figures 2 – 5 illustrate the relationships of shear stress and shear strain. The stress paths were shown in Figures 6 – 9. Shear stress, τ and shear strain, γ were calculated from the following equations;

$$\tau = (\sigma_a - \sigma_r)/2 \quad (1)$$

$$\gamma = \varepsilon_a - \varepsilon_r = 1.5\varepsilon_a \quad (2)$$

$$p' = (\sigma'_a + 2\sigma'_r)/3 \quad (3)$$

where σ_a and σ_r were axial and radial stress, ε_a and ε_r were axial and radial strains. p' was the mean effective principal stress. The recovery of shear stiffness was observed due to cyclic mobility in all the tests, since the middle dense sand with a relative density of 70 % was tested. Phase transformation lines were also clearly observed in the stress paths.

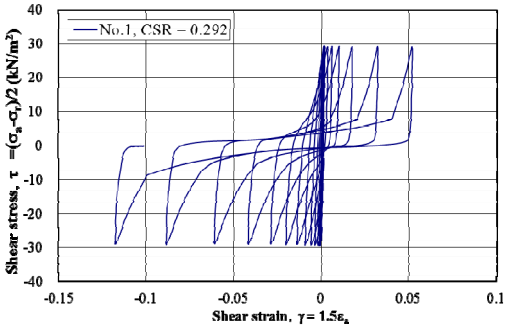

Figure 2. Stress-strain relationship in No.1.

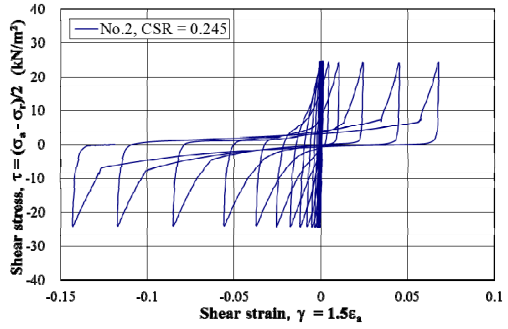

Figure 3. Stress-strain relationship in No.2.

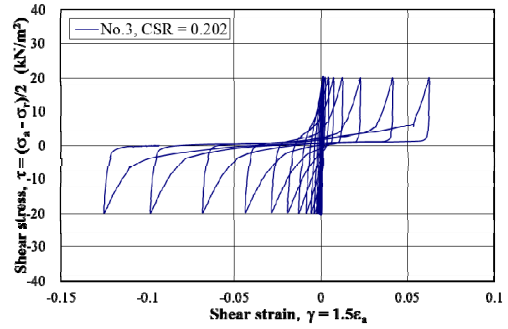

Figure 4. Stress-strain relationship in No.3.

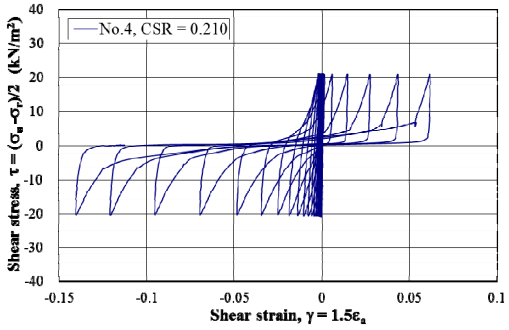

Figure 5. Stress-strain relationship in No.4.

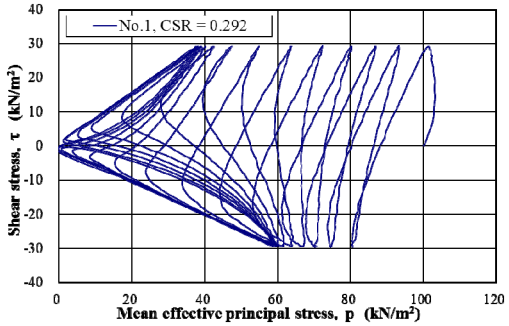

Figure 6. Stress path in No.1.

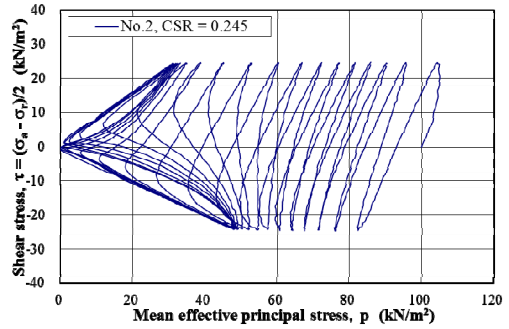

Figure 7. Stress path in No.2.

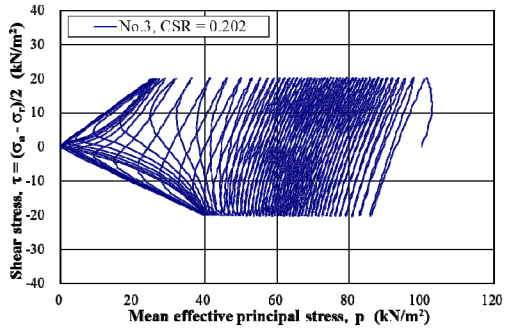

Figure 8. Stress path in No.3.

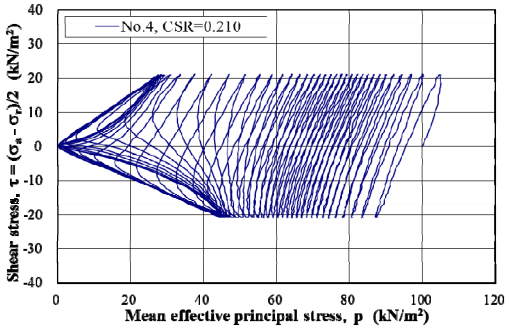

Figure 9. Stress path in No.4.

The dissipation energy in one cycle of loading, ΔU and the accumulated dissipation energy in the n-th cycle, U_n were calculated from Equations (4) and (5).

$$\Delta U = \int \tau \cdot d\gamma \tag{4}$$

$$U_n = \sum_{i=1}^{n} \Delta U_i \tag{5}$$

The relationship of excess pore pressure ratio and the accumulated dissipation energy are shown in Figure 10. Double amplitudes of axial strain are also plotted against the dissipation energy in Figure 11. In Figures 10 and 11, these relationships were unfortunately different from each other. With the increase of cyclic stress ratio (CSR), the dissipation energy was increased at the same values of excess pore pressure ratio and axial strain. The reason for this is that the cyclic mobility was induced during the cyclic loading, and that the dissipation energy got larger due to the cyclic mobility with the increase of cyclic stress ratio. That is, the dissipation energy due to the cyclic mobility did not develop excess pore pressure and deformation. Therefore, it is necessary to adjust the dissipation energy in some way for evaluating liquefaction potential of the middle dense sand using the energy-based method.

In general, the dissipation energy has been often normalized by the confining pressure during consolidation as well as the shear stress ratio. But the effective confining pressure in a cycle always changes with the increase of excess pore pressure. The authors tried to normalize the dissipation energy by the effective confining pressures at the beginning of each cycle. Figures 12 and 13 plot the excess pore pressure ratios and the axial strains against the normalized dissipation energy that is divided by the confining pressures at the beginning of each cycle. The excess pore pressures ratio were agreed with each other, but the double amplitudes of axial strain were different.

Next, the shear stress was also divided by the effective confining pressure at the beginning of each cycle to calculate the shear stress ratio. The shear stress ratios are plotted against the increment of the normalized dissipation energy in Figure 14. It was found from Figure 14 that the shear stress ratio at each cycle correlated with the increment of the normalized dissipation energy. In other words, this figure suggests that both of the stress-based and the energy-based methods are basically same in evaluating liquefaction potential. Additionally, an interesting behavior was observed in the early stage of Figure 14. Figure 15 shows the magnified view of the relationship between the shear stress ratio and the increment of normalized dissipation energy. In the case of No.3 and 4 with a smaller cyclic stress ratio, the increment of normalized dissipation energy decreased with the increase of cycle's number. The behavior indicates that soils got stiffer by the small and cyclic loads even in the undrained condition, and may be useful for investigating aging effects on a liquefaction resistance.

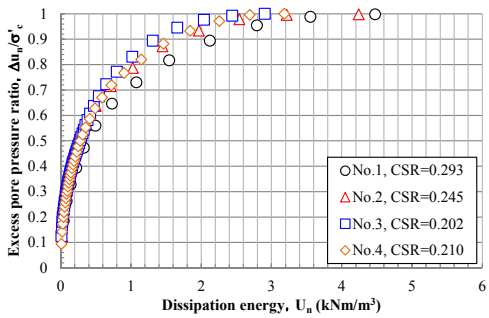

Figure 10. Relationships of dissipation energy and excess pore pressure ratio.

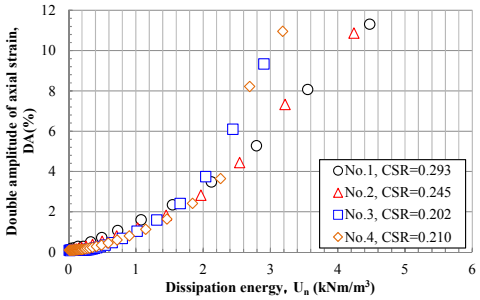

Figure 11. Relationships of dissipation energy and double amplitude of axial strain.

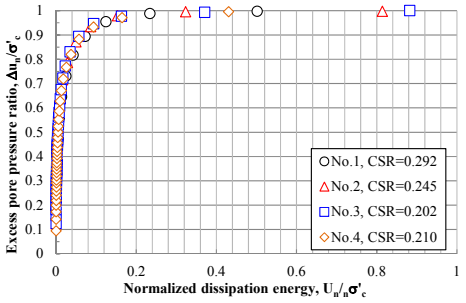

Figure 12. Relationships of normalized dissipation energy and excess pore pressure.

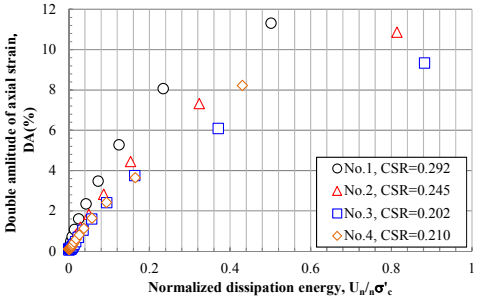

Figure 13. Relationships of normalized dissipation energy and double amplitude of axial strain.

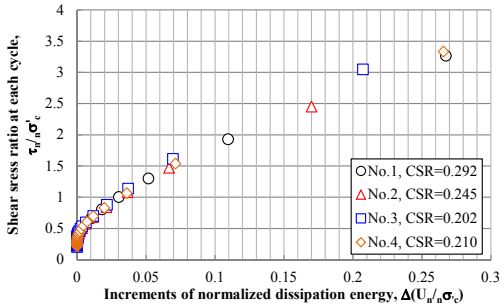

Figure 14. Shear stress ratios and increments of normalized dissipation energy using confining pressure at the beginning of each cycle.

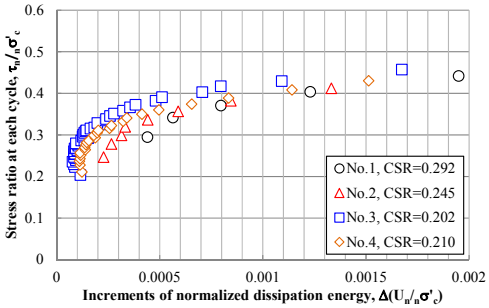

Figure 15. Magnified view of the relationship of shear stress ratio and normalized dissipation energy in early stage of tests.

4 SIMULATION OF LIQUEFACTION STRENGTH CURVE

Using the relationships in Figures 12 and 14, it is possible to simulate the development of excess pore pressure under cyclic loading with arbitrary cyclic stress ratios, and reproduce the number of cycles reaching an excess pore pressure ratio of 0.95. That is, a liquefaction strength curve can be obtained from a single test. The flow chart to calculate a liquefaction strength curve is shown in Figure 16. In this flow chart, it is necessary to estimate the confining pressure in the next cycle, because the final excess pore pressure in a cycle is often different from the maximum one. The relationship of the normalized dissipation energy and the excess pore pressure ratio at the beginning of next cycle was used as it is shown in Figure 17.

To verify the new method in estimating a liquefaction curve, the results of cyclic undrained triaxial tests were inspected. Figure 18 shows the four estimated liquefaction strength curves and the four test results as a symbol of black circle. It can be seen in Figure 18 that the four estimated curves were agreed with each other, since the four specimens had the same physical properties, and that they could reproduce the test results in the range of 0.202 to 0.293 in the cyclic stress ratio. This method has the benefit of evaluating the liquefaction resistance in a wide range of the cyclic stress ratio, because the increment of normalize dissipation energy was related to the shear stress ration with the wide range as seen in Figure 14. A logarithm interpolation shown in Figure 19 was adopted for very low cyclic stress ratios to consider the influence that the specimens got stiffer by small cyclic loading (Figure 15). Comparing a scatter of test results, the specimens of No.2 and 4 with the relatively low velocity of S wave showed low liquefaction strength curves. This method can be also useful in quantitatively evaluating a scatter of collected specimens from a natural deposit ground.

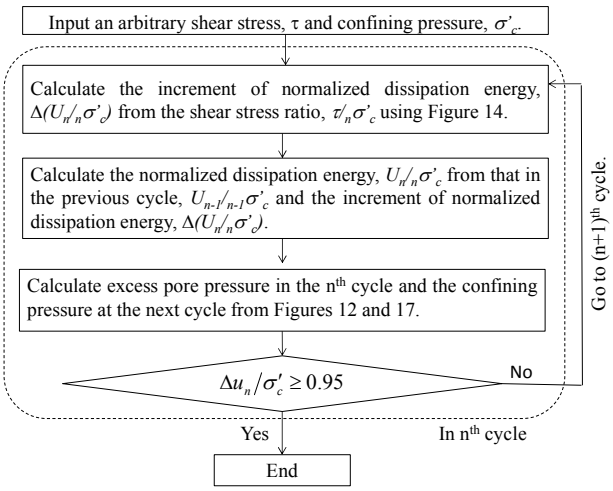

Figure 16. Flow chart to calculate a liquefaction strength curve using a cyclic undrained triaxial test.

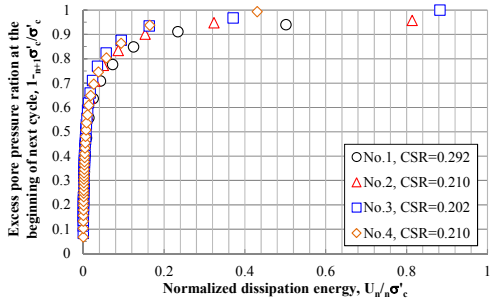

Figure 17. Relationships of normalized dissipation energy and excess pore pressure ratio at the beginning of next cycle.

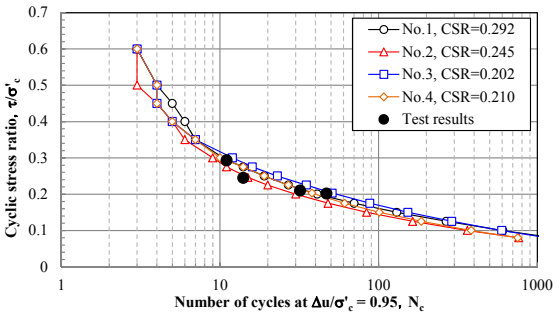

Figure 18. Estimated liquefaction strength curves and test results of cyclic undrained triaxial tests.

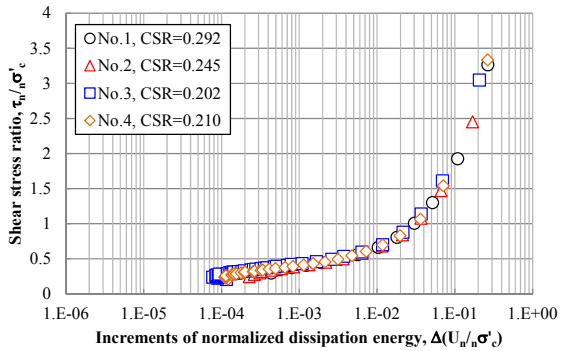

Figure 19. Relationship of shear stress ratio and normalized dissipation energy in a logarithm scale.

5 CONCLUSIONS

This paper conducted a series of cyclic undrained triaxial tests and proposed a new method to estimate a liquefaction strength curves from a cyclic undrained triaxial tests using the concept of energy dissipation. The following conclusions were obtained,

1) The shear stress ratio and the increment of normalized dissipation energy divided by the confining pressure at the beginning of each cycle had a particular relationship. The stress-based and energy-based methods in evaluating liquefaction potential are basically same.
2) The new method could reproduce the liquefaction resistances in the cyclic undrained triaxial tests, and could give liquefaction strength curves in a wide range of cyclic stress ratio.
3) The new method also makes it possible to evaluate a scatter of specimens comparing liquefaction strength curves, which is useful in improving the accuracy of numerical simulation on predicting liquefaction of a natural deposit ground.

6 REFERENCES

Towhata I. and Ishihara K. 1985. Shear work and pore pressure in undrained shear, *Soils and Foundations* 25 (3), 73-84.

Kazama M., Yamaguchi A. and Yanagisawa E. 2000. Liquefaction resistance from a ductility viewpoint, *Soils and Foundations* 40 (6), 47-60.

Kokusho T. and Mimori Y. 2015. Liquefaction potential evaluations by energy-based method and stress-based method for various ground motions, *Soil Dynamics and Earthquake Engineering* 75, 130–146.